Biochimica et Biophysica Acta, 1102 (1992) 202–212

BBABIO 43692

Ultrafast energy transfer in LHC-II trimers from the Chl *a*/*b* light-harvesting antenna of Photosystem II

Stefan L.S. Kwa [b], Herbert van Amerongen [a], Su Lin [a], Jan P. Dekker [b], Rienk van Grondelle [b] and Walter S. Struve [a]

[a] *Ames Laboratory-USDOE and Department of Chemistry, Iowa State University, Ames, IA (USA) and* [b] *Department of Physics and Astronomy, Free University, Amsterdam (Netherlands)*

(Received 20 February 1992)
(Revised manuscript received 4 May 1992)

Key words: Antenna; Chlorophyll; Light-harvesting complex; Photosystem II; Plant photosynthesis; Pump-probe spectroscopy; Ultrafast spectroscopy

Time-resolved absorption difference profiles were obtained for LHC-II trimers, isolated from Photosystem II in spinach with n-dodecyl β-D-maltoside, using one-color and two-color pump-probe techniques. The one-color isotropic signals are predominantly excited state absorption at 640 nm, and a combination of photobleaching and stimulated emission at wavelengths ≥ 665 nm. At intermediate wavelengths, dynamic red-shifting due to downhill energy transfer among the chlorophyll (Chl) spectral forms produces a bipolar signal, in which prompt photo-bleaching/stimulated emission is superseded at later times by excited state absorption. Triexponential analyses of these profiles yield the lifetime components 2–6 ps (associated with the spectral shifting), 14–36 ps (possibly due to energy transfer between LHC-II monomers), and several hundred picoseconds. The one-color anisotropy decays are resolvable at 665–675 nm, with lifetimes of 4.3 to 6.3 ps. They are unresolvably fast (i.e., exhibit subpicosecond lifetimes) at 640–650 nm. The two-color isotropic absorption difference signals show clear spectral evolution arising from equilibration among the LHC-II spectral components for excitation wavelengths shorter than 670 nm. However, most of this spectral evolution occurs within less than 2.5 ps. No resolvable anisotropy decay was observed in the two-color experiments. Taken together, the one-color and two-color experiments indicate that both picosecond and subpicosecond energy transfer steps occur in this antenna. The faster processes appear to dominate the spectral equilibration; slower processes occur in isoenergetic energy transfers among the longer-wavelength Chl *a* spectral forms that absorb between 665 and 675 nm. The values of the long-time anisotropies $r(\infty)$, measured in the one-color and two-color experiments, are qualitatively consistent with static linear dichroism spectra of these preparations.

Introduction

The light-harvesting Chl *a*/*b* complex LHC-II, associated with Photosystem II, contains about 50% of all chlorophyll chromophores synthesized in green plants and green algae. It serves as the principal antenna for solar energy, it is involved in the stacking of thylakoid membranes, and it mediates the energy allocation between Photosystems I and II [1]. The LHC-II complex is organized into trimers containing 27 kDa and 25 kDa apoproteins. While these apoproteins differ in phosphorylation potentials, they exhibit considerable sequence homology, and bind essentially identical organizations of chlorophyll molecules [2,3]. Electron diffraction, microscopy, and imaging studies of this complex have progressively revealed more detailed information about its symmetry and protein conformation since 1983 [4–6]. These experiments culminated in a recent 6 Å resolution electron crystallography study [7], which disclosed for the first time the positions and approximate orientations of the 15 chlorophyll pigments in an LHC-II monomer.

The new structural data have in turn prompted reexamination of the low-temperature spectroscopic properties [8] in trimers solubilized with n-dodecyl β-D-maltoside. The Chl *a*/*b* ratio in these preparations is ca. 1.5, indicating that the protein monomer probably contains 9 Chl *a* and 6 Chl *b* chromophores. The spectroscopy of these trimers closely resembles

Correspondence to: W. Struve, Department of Chemistry, Iowa State University, Ames, IA 50011, USA.

Abbreviations: BChl, bacteriochlorophyll; CD, circular dichroism; Chl, chlorophyll; EET, electronic excitation transfer; ESA, excited state absorption; fwhm, full width at half maximum; LD, linear dichroism; LHC-II, light-harvesting complex from Photosystem II; *A*, absorbance.

that of intact thylakoid membranes [8], but differs somewhat from that of LHC-II isolated in Triton X-100 [9]. This suggests that the LHC-II complex in the newer isolations, using the gentler detergent, may be more physiological. Analysis of low-temperature absorption, LD, and CD spectra indicated that the Chl *a*/*b* Q_y absorption spectrum in LHC-II trimers comprises at least six different spectral components. Polarized fluorescence excitation spectra show evidence of efficient energy equilibration among the red-most Chl *a* pigments responsible for the 676 nm spectral component. The CD spectrum indicates the presence of strong exciton interactions among the Chl *a* and Chl *b* chromophores, as is to be expected in view of the small nearest-neighbor separations (9–14 Å) found in LHC-II [7].

Previous ultrafast studies of LHC-II energy transfer include two transient absorption studies [10,11] and a subpicosecond fluorescence upconversion experiment [12]. These two approaches have yielded very different views of the energy transfer time scales. The Chl *b* → Chl *a* and Chl *a* → Chl *a* energy transfer times derived from pump-probe measurements on a Triton X-100 LHC-II preparation were 6 ± 4 ps and 20 ps, respectively [10]. In these experiments, the Chl *b* → Chl *a* energy transfer kinetics were inferred from isotropic photobleaching decay in the Chl *b* absorption region, where no depolarization was found. The Chl *a* → Chl *a* kinetics were determined from one-color anisotropy decay at 665 nm. Gillbro et al. [11] later inferred a nearest-neighbor energy transfer time of 5 ps at most (and probably closer to 1 ps) on the basis of exciton annihilation kinetics in aggregates of Chl *a*/*b* complexes from spinach. The Chl *a* fluorescence rise-time observed by Eads et al. [12] upon 650 nm excitation of Chl *b* in the LHC-II antenna of a *C. reinhardtii* strain deficient in Photosystems I and II indicated a Chl *b* → Chl *a* transfer time on the order of 500 fs. The latter group speculated that the lower time resolution and the presence of the coherent coupling artifact [13] in the one-color pump-probe studies [10] may have obscured subpicosecond energy transfer processes. Triton X-100 solubilization may also decouple significant numbers of Chl *a* pigments from other chromophores, introducing slow processes that are absent in the intact antenna.

In the present work, we report one- and two-color pump-probe experiments on LHC-II trimers isolated using n-dodecyl β-D-maltoside. These appear to be timely for several reasons. First, the newly discovered LHC-II structure [7] has supplanted earlier models [14–16] of its chromophore organization, so that experiments can be targeted toward understanding structure-function relationships. Second, the confirmation that our preparations are spectroscopically similar to those of LHC-II in situ [8] enables us to gauge the possible effects of solubilization on the earlier kinetic experiments. Finally, one- and two-color pump-probe techniques can yield very different perspectives on the energy transport (depending on the chromophore architecture), so that the origins of the contrasting results in the one-color experiments [10,11] and the fluorescence upconversion work (inherently a two-color technique) may be more fundamental than previously envisaged.

Materials and Methods

The isolation of the LHC-II trimers using n-dodecyl β-D-maltoside has been described earlier [8]. PS-II membrane fragments were obtained from spinach thylakoids as reported by Berthold et al. [17], and solubilized with 1% (w/v) n-dodecyl β-D-maltoside in a buffer of 20 mM BisTris, 20 mM $MgCl_2$, 10 mM $MgSO_4$, and 5 mM $CaCl_2$ at pH 6.5. The solubilized fraction was loaded onto a Q-Sepharose column equilibrated with the same buffer as described above, but with 0.03% dodecylmaltoside. These buffer conditions allowed retention of the Photosystem II core complex, but not of LHC-II [18]. The LHC-II enriched eluate was centrifuged on a linear sucrose gradient at 4°C in a Beckman SW 41 rotor at 41000 rpm for 16 h. The purified LHC-II was verified by SDS-PAGE to consist of 25 and 27 kDa polypeptides. The Q_y absorption spectra of the LHC-II preparations conformed to those reported in Ref. 8. Samples were stored in the dark near 0°C. Room-temperature experiments were conducted with samples in a buffer of 20 mM Bistris with 20 mM NaCl and 0.03% dodecylmaltoside at pH 6.5. These samples exhibited about 0.4 *A* at 676 nm in Starna 49-G1 1 mm path length cells, which were periodically translated over ca. 2 cm at 2 Hz to minimize laser photooxidation. The room temperature Q_y absorption spectrum of the LHC-II trimers is shown in Fig. 1.

The lasers and pump-probe apparatus have been described previously [19]. The principal modification was the addition of a second hybrid mode-locked dye laser for two-color studies. Both dye lasers (DCM laser dye, DDCI saturable absorber dye) were pumped using 532 nm SHG pulses (70 ps fwhm, approx. 1 W average power) from a Nd:YAG cw mode-locked laser. Each dye laser typically exhibited autocorrelations with about 3–4 ps fwhm, and was tunable from 640 to 680 nm. The dual laser cross-correlation (evaluated with a Type I $LiIO_3$ SHG crystal in place of the sample) varied with wavelength, but was typically 5–8 ps fwhm. In an RF multiple-modulation scheme, the pump and probe beams were modulated at 6.5 and 0.5 MHz, respectively in Isomet 1206-C acousto-optic modulators. The pump pulse delay was swept using a retroreflector mounted on a Micro-Controle UT100125PP translation

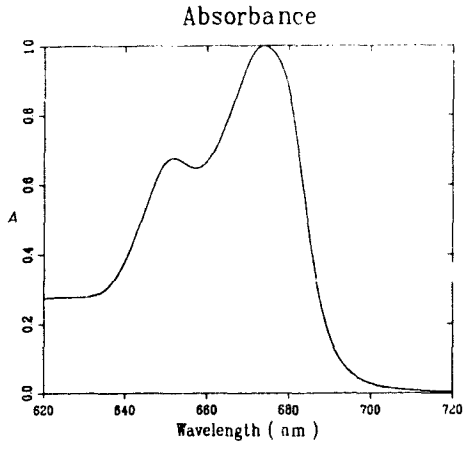

Fig. 1. Q_y absorption spectrum of LHC-II trimers in a pH 6.5 solution containing 20 mM Bistris, 20 mM NaCl, 0.03% (w/v) dodecyl maltoside, and 70% (w/v) glycerol. Spectral resolution is 1 nm.

stage. Both beams were focussed into the sample with a 7 cm f.l. lens, and the transmitted probe beam was detected with a 0.51 mm^2 EG&G FOD-100 silicon photodiode. The probe beam polarization was fixed at 45° from the vertical laser polarization. The polarization of the pump beam was defined by a rotatable Glan-Thompson prism. In a recent study that compared time-resolved anisotropy decays with static LD measurements in the BChl *c* antenna in chlorosomes from *Chloroflexus aurantiacus*, it was determined that the ratio of the two polarized pump beam intensities in pump-probe experiments was moderately wavelength-dependent [20]. The difference signals for different polarizations were, therefore, normalized to the respective pump and probe beam intensities at every wavelength. The 7.0 MHz sum frequency component in the absorption difference signal was recovered in a Drake R-7A radio receiver, whose signal-bearing 50 kHz intermediate frequency was fed into a Stanford Research Systems SR510 lock-in amplifier. In some experiments, the pump-probe profiles were also normalized to the real-time laser intensity. Profiles were accumulated in a DEC MINC-23 computer, and transferred to a DEC VAXstation 2000 for analysis with nonlinear least-squares convolute-and-compare algorithms. For all combinations of pump and probe wavelengths, polarized profiles $\Delta A_{\parallel}(t)$ and $\Delta A_{\perp}(t)$ were obtained with parallel and perpendicular polarizations respectively. The isotropic decay functions $\Delta A(t)$ were then computed from

$$\Delta A(t) = \Delta A_{\parallel}(t) + 2\Delta A_{\perp}(t) \qquad (1)$$

while the anisotropy functions $r(t)$ were evaluated from

$$r(t) = \frac{\Delta A_{\parallel}(t) - \Delta A_{\perp}(t)}{\Delta A(t)} \qquad (6)$$

The maximum number of photons absorbed per chromophore per laser pulse in the overlap region of the pump and probe pulses was about 0.01 at 676 nm. The effects of exciton annihilation on the isotropic decay kinetics were studied by varying the pump beam intensity over two orders of magnitude (vide infra).

Results

One-color experiments

Representative isotropic absorption difference profiles obtained in one-color experiments at six wavelengths from 640 to 675 nm are shown in Fig. 2. The principal features of these transients are as follows: (a) At the shortest wavelength studied (640 nm), the (positive) signal is dominated at all times by excited state absorption (ESA). At the two longest wavelengths (665 and 675 nm), the (negative) signal is principally a combination of photobleaching and stimulated emis-

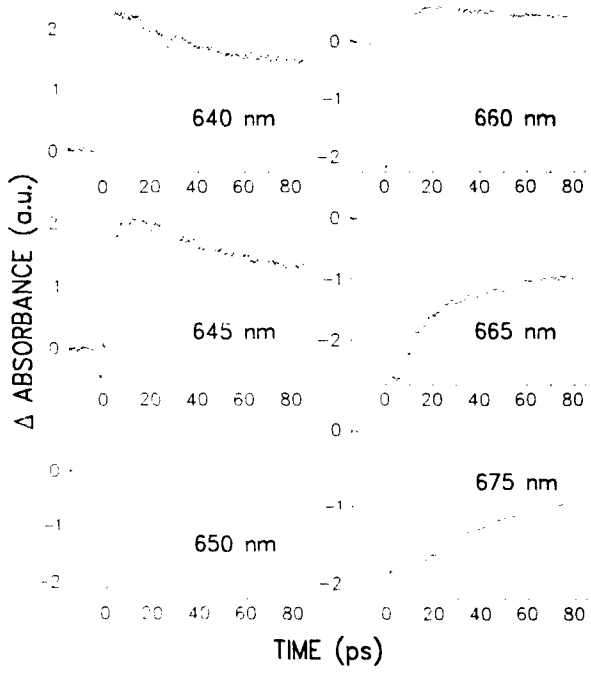

Fig. 2. One-color isotropic absorption difference profiles at six wavelengths from 640 to 675 nm. Positive and negative signals correspond to excited state absorption and photobleaching/stimulated emission, respectively. Final parameters for triexponential fits to these and other isotropic profiles are given in Table 1. The profiles at different wavelengths are not mutually normalized.

sion throughout. At intermediate wavelengths (645–660 nm), a prompt photobleaching signal gives way to ESA within ≤ 5 ps. The dichotomy between the ESA and photobleaching observed at the shortest and longest wavelengths, respectively, can be phenomenologically rationalized in terms of Chl *a* ground and Q_y excited state absorption spectra qualitatively similar to those that have been recently characterized for BChl *a* monomers by Parson and co-workers [21]. For BChl *a* in methanol, the integrated ESA spectrum is similar to the integrated ground state spectrum; the ESA spectrum is considerably broader, and exhibits a maximum absorption coefficient is at most half that of the ground state spectrum. Hence, the net signal at wavelengths considerably to the blue of the LHC-II Q_y absorption band should be dominated by ESA (assuming that the relationships between the Chl *a*/*b* ESA and ground state spectra are similar to those in BChl *a*). This is also consistent with absorption difference spectra observed by Shepanski and Anderson [22] for Chl *a* monomers in pyridine: at long times, the latter spectra show ESA and photobleaching/stimulated emission, respectively, at wavelengths less than, and greater than, about 655 nm. The bipolarity of our absorption transients at the intermediate wavelengths must arise from dynamic spectral shifting, stemming from energy transfer among different Chl *a*/*b* spectral components [8]. We caution here that the details of the Chl *a*/*b* absorption difference spectra in LHC-II may differ from those of the monomeric pigments in consequence of exciton couplings [8] and/or pigment-protein interactions. (b) Triexponential fitting of the isotropic transients yields three families of lifetimes that are essentially uniform (with minor fluctuations) across the wavelength spectrum. In this analysis, the gross wavelength variations apparent in the profiles shown in Fig. 2 arise from redistributions in the pre-exponential factors. The lifetime groups evident in Table I are (i) 2–6 ps; (ii) 14–36 ps; and (iii) several hundred picoseconds. The latter (longest) lifetime components are less accurately determined than the others, because the sweep duration was typically limited to 80 ps. The first family of lifetimes (2–6 ps) arises from spectral shifting, and corresponds to the time scale of the bipolar switching at the intermediate wavelengths, 645–660 nm. The intermediate lifetimes (14–36 ps) may result from EET between monomers within a trimer, because it resembles a lifetime component that emerges in exciton annihilation studies of the isotropic decay (see below). (c) Annihilation effects were screened by reducing the pump pulse intensities by factors of 10 and 10^2 below those used in the isotropic studies of Fig. 2, with the results shown in Fig. 3 and Table II. (In Fig. 2, the total pulse intensity was about $3 \cdot 10^{13}$ photons cm^{-2}, distributed in an approx. 2:1 ratio between pump and probe pulses; this

TABLE I

Fitting parameters from triexponential analyses of one-color isotropic decays in LHC-II

All lifetimes are in ps.

Wavelength (nm)	$\tau_1(A_1)$	$\tau_2(A_2)$	$\tau_3(A_3)$
640	5.3 (−0.27)	16 (0.32)	450 (0.42)
645	5.6 (−0.40)	18 (0.26)	270 (0.35)
	4.0 (−0.48)	17 (0.18)	342 (0.33)
650	4.4 (−0.76)	15 (0.06)	200 (0.18)
	4.2 (−0.78)	22 (0.07)	223 (0.15)
655	4.7 (−0.78)	14 (0.06)	215 (0.16)
660	3.7 (−0.88)	19 (0.05)	112 (0.07)
	3.6 (−0.85)	19 (0.05)	239 (0.10)
665	2.9 (−0.60)	23 (−0.24)	1.5E6 (−0.15) [a]
	3.0 (−0.73)	27 (−0.13)	536 (−0.14)
	2.5 (−0.69)	26 (−0.15)	352 (−0.16)
670	3.8 (−0.26)	31 (−0.37)	256 (−0.37)
	3.6 (−0.30)	36 (−0.28)	249 (−0.42)
675 [b]		20 (−0.47)	250 (−0.53)
		26 (−0.41)	144 (−0.59)

[a] Limited fitting interval.

[b] Biexponential fits are used at 675 nm, as their quality is similar to that of triexponential fits.

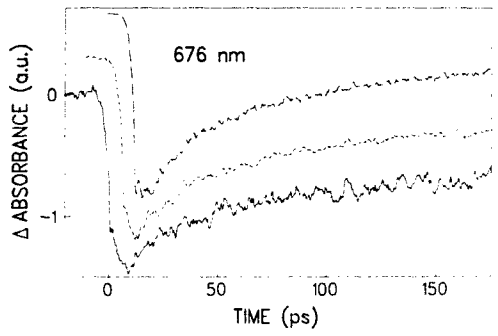

Fig. 3. One-color isotropic absorption difference profiles at 676 nm for 100%, 10%, and 1% excitation power (top, middle, and bottom respectively). The signal at this wavelength is dominated by Chl *a* photobleaching/stimulated emission. The profiles are not mutually normalized. Optimized parameters for biexponential and triexponential fits to these profiles are listed in Table II.

TABLE II

Effect of pump power on one-color isotropic decays at 675 nm: biexponential and triexponential fits

All lifetimes are in ps.

Percent laser power	$\tau_1(A_1)$	$\tau_2(A_2)$	$\tau_3(A_3)$
1	0.31 (−0.77)	22 (−0.09)	447 (−0.14)
	20 (−0.41)	443 (−0.59)	
10	0.46 (−0.83)	24 (−0.07)	380 (−0.10)
	21 (−0.47)	205 (−0.53)	
100	0.46 (−0.83)	22 (−0.08)	259 (−0.09)
	20 (−0.52)	272 (−0.48)	

corresponded to approx. one excitation per four trimers.) The ground-state recovery is visibly faster at the higher pump pulse intensities in Fig. 3. These decays, obtained with 160 ps sweep durations near the 676 nm Chl *a* photobleaching maximum, were analyzed with biexponential and triexponential model functions. The biexponential analyses indicate a 20 ps fast component, whose contribution increases with laser intensity. However, the triexpoential analyses show that such a simple correlation can be spurious: here, the contribution of the 20 ps component is slightly higher at 1% laser intensity than at 10% intensity. Hence, direct comparisons of preexponential factors in the 20 ps component can be misleading, due to simultaneous changes in the other lifetime components. The principal conclusion that can be drawn here is that there is an intensity-dependent component, with a lifetime in the low tens of picoseconds, which makes a substantial contribution even at 1% laser intensity. At such laser powers (about 1 excitation per 400 trimers), singlet-singlet annihilation is highly improbable. Isotropic lifetime components cannot arise from energy equilibration between spectrally identical chromophores; the 20 ps process could originate, in principle, from energy transfer between chromophores in contrasting protein environments (e.g., bound to 25 and 27 kDa apoproteins within a trimer, or located in similar proteins but exhibiting spectral inhomogeneity). More detailed examination of this lifetime component at 300 and 23 K (H. Van Amerongen, S.L.S. Kwa, H.-C. Chang, J.P. Dekker, R. van Grondelle and W.S. Struve, unpublished work) suggests that it arises principally from singlet-triplet annihilation, resulting from triplet state buildup (e.g., in the carotenoids) that accumulates over a large number of laser pulses.

Anisotropic one-color profiles are shown in Fig. 4 for several wavelengths. At 640 nm, the depolarization

TABLE III

One-color anisotropy decay parameters for LHC-II [a]

Wavelength (nm)	$r(0)$	$r(\infty)$	τ(ps)
640		-0.01 ± 0.03	
645		-0.03 ± 0.13	
650		-0.03 ± 0.03	
655		-0.05 ± 0.04	
660		-0.03 ± 0.03	
665	0.22	0.05 ± 0.04	6.3 ± 2.0
670	0.13	0.02 ± 0.03	5.0 ± 2.0
675	0.14	0.00 ± 0.03	4.3 ± 2.0

[a] Values for $r(0)$ and τ are listed only for wavelengths at which resolvable depolarization lifetime components were observed.

is clearly faster than the time resolution of 3–4 ps, because the derived anisotropy function (not shown) is essentially constant at times beyond the coherent laser spike (In this regard, our anisotropy decays at 640–655 nm resemble the 652 nm anisotropy described by Gillbro et al. [10], although our measured anisotropies are much smaller than the value 0.42 ± 0.05 reported by these authors at 652 nm.) At the three longest wavelengths, however, discernible anisotropy decay sets in, with a lifetime of about 6 ps at 665 nm and about 4 to 5 ps at 670 and 675 nm. The depolarization lifetimes and residual anisotropies are shown for these and several other wavelengths in Table III. A careful comparison was made between the anisotropy decay and the instrument function at 675 nm in order to address the effects of the coherent spike, with the results shown in Fig. 5. The shown anisotropy decay $r(t)$ is an average from five pairs of measurements of $\Delta A_{\parallel}$, $\Delta A_{\perp}$. The decay in $r(t)$ exhibits a lifetime component (4.3 ps) that is clearly not attributable to the instrument function wing. Moreover, one-color anisotropy decays obtained using independent lasers tuned to the same wavelength (which do not produce a coherent spike because the

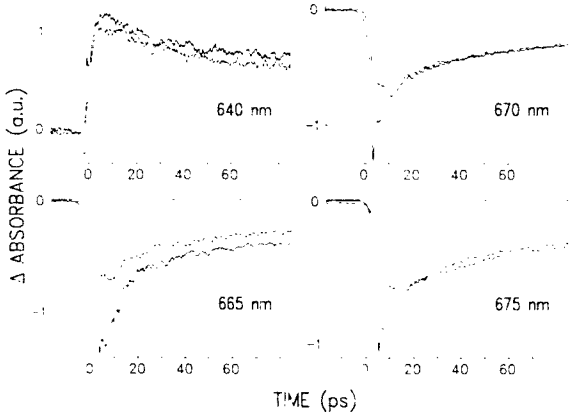

Fig. 4. One-color anisotropic absorption difference profiles $\Delta A_{\parallel}(t)$, $\Delta A_{\perp}(t)$ at 640, 665, 670 and 675 nm. Fitting parameters are given for these and other anisotropic profiles in Table III.

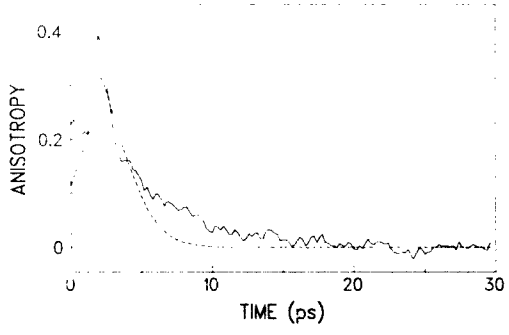

Fig. 5. One-color anisotropy decay function $r(t)$ at 675 nm, superimposed on the corresponding instrument function (symmetric curve). The anisotropy decay is averaged over five pairs of profiles $\Delta A_{\parallel}(t)$, $\Delta A_{\perp}(t)$ at this wavelength. The corresponding anisotropy decay time, derived from a single-exponential fit, is 4.3 ps.

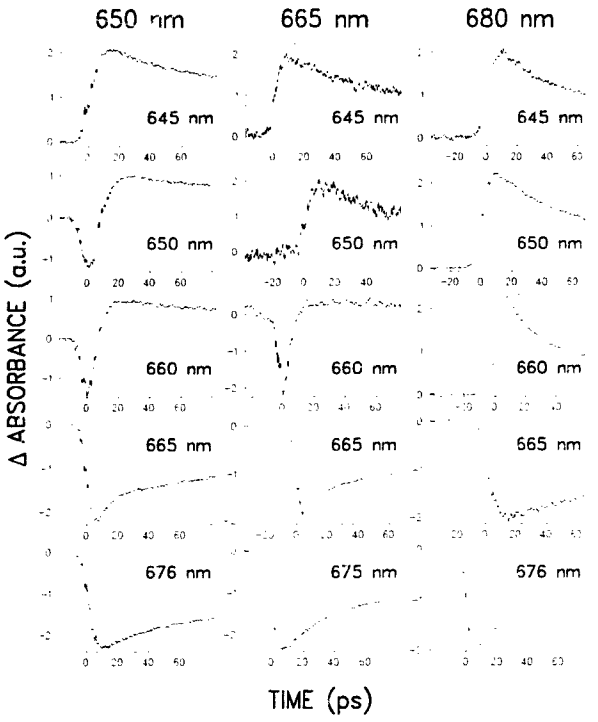

Fig. 6. Two-color isotropic absorption difference profiles excited at 650, 665, and 680 nm (first, second, and third columns, respectively), and probed at several wavelengths from 645 to 676 nm. Final parameters for biexponential fits to these and other profiles are given in Table IV. Profiles at different wavelengths are not mutually normalized. The position of zero time (coincidence between pump and probe pulses) changes with wavelength, because time delay between 532 nm YAG laser pulse and dye laser pulse is sensitive to dye laser wavelength.

lasers exhibit uncorrelated noise patterns) are similar to those generated using a single laser.

Two-color experiments

Some appreciation of the spectral information afforded by two-color isotropic profiles for LHC-II may be gained by comparing transients obtained at contrasting excitation wavelengths. These are shown in Fig. 6 for the wavelengths 650 nm (which predominantly excites Chl *b* spectral components) and 665 and 680 nm (which are in the Chl *a* absorption region). These three groups of profiles resemble each other (and the one-color profiles in Fig. 2) in that the absorption difference signal is dominated by ESA at the shortest probe wavelength (645 nm) and by photobleaching and stimulated emission at the longest wavelengths (665–675 nm). When the pump wavelength is detuned from the probe wavelength (transforming a one-color into a two-color experiment), the resulting isotropic profile will differ from the one-color profile if spectral equilibration is incomplete on the experimental timescale. Comparisons between the one-color and two-color profiles in Figs. 2 and 6 reveal striking examples of such contrasts. As expected, the one-color 650 nm profile in Fig. 2 resembles the two color profile excited and probed at 650 nm in Fig. 6. It bears little resemblance to the two-color profiles probed at 650 nm after excitation at either 665 or 680 nm; the prompt, short-lived photobleaching signal that appears under 650 nm pumping is absent at the other two pump wavelengths. Similarly, the one-color 665 nm profile (Fig. 2) is comparable to the two-color profile excited and probed at 665 nm (Fig. 6). It differs considerably from the two-color profiles probed at 665 nm after either 650 or 680 nm excitation, in that the former profile exhibits a visibly larger fast decay component (lifetime < 5 ps) in the photobleaching/stimulated emission signal. (This dissimilarity is especially conspicuous between the profiles excited at 665 and 680 nm.) These examples illustrate that one-color isotropic profiles generated by exciting higher-energy spectral forms can exhibit large photobleaching decay components, attributable to equilibration with lower-energy spectral forms. This serves as a caveat for the interpretation of one-color isotropic profiles in antennae that are connected to an excitation trap (e.g., the Photosystem I core antenna). In such systems, fast photobleaching decay components at the blue edge of the antenna spectrum may stem from spectral equilibration rather than trapping. For all of the excitation wavelengths in Fig. 6, the photobleaching decays exhibit progressively smaller amplitudes of fast decay components as the probe wavelength is increased from 665 to 675 nm. Optimized parameters are given for biexponential fits to these and other two-color isotropic profiles in Table IV.

An additional perspective is gained by organizing the isotropic transients obtained at different probe wavelengths into absorption difference spectra for fixed time delays. In Fig. 7, we plot the absorption differences computed from optimized triexponential fits to the isotropic decays for several probe wavelengths between 645 and 674 nm under 650 nm excitation. Plotting these fits instead of the original curves deconvolutes them from the instrument functions, which vary with wavelength. Absorption difference signals $\Delta A(\lambda)$ for different probe wavelengths λ were mutually normalized using

$$\Delta A(\lambda) = \frac{S(\lambda)}{I_{\text{pump}}(650\text{ nm})\, I_{\text{probe}}(\lambda)\, 10^{-D(\lambda)}} \tag{3}$$

where I_{pump}, I_{probe} are the relevant laser intensities, $S(\lambda)$ is the measured absorption difference signal, and $D(\lambda)$ is the sample optical absorbance. In this figure, the prompt (0 ps) difference spectrum consists principally of a photobleaching-stimulated emission peak at 650 nm, indicating that most of the immediate signal arises from LHC-II pigments that are (nearly) isoener-

TABLE IV

Fitting parameters for biexponential fits to two-color isotropic decays in LHC-II

All lifetimes are in ps. These biexponential fits do not reveal the full range of lifetimes contained in the isotropic decays, and are intended only to convey the gross wavelength variations in the isotropic profiles. Triexponential fits to the profiles excited at 650 nm and probed at 665–676 nm, for example, reveal a very fast photobleaching-stimulated emission rise component that corresponds to downhill excitation transport among Chl spectral forms (cf. Fig. 7).

Pump wavelength (nm)	Probe wavelength (nm)	$\tau_1(A_1)$	$\tau_2(A_2)$
650	645	18 (0.10)	221 (0.90)
	650	5.4 (−0.83)	182 (0.17)
	655	6.6 (−0.70)	193 (0.30)
	660	4.5 (−0.84)	208 (0.16)
	665	5.7 (−0.51)	228 (−0.49)
	670	7.2 (−0.61)	231 (−0.59)
	676	20 (0.16)	262 (−0.84)
665	645	24.8 (0.29)	178 (0.71)
	650	8.3 (−0.21)	86 (0.79)
	655	4.0 (−0.65)	90 (0.35)
	660	4.4 (−0.97)	56 (0.03)
	665	4.7 (−0.62)	136 (−0.38)
	670	15 (−0.37)	127 (−0.63)
	675	30 (−0.54)	380 (−0.46)
680	645	17 (0.29)	116 (0.71)
	645	35 (0.25)	105 (0.75)
	650	23 (0.28)	129 (0.72)
	655	14 (0.40)	116 (0.60)
	660	7.4 (0.45)	74 (0.55)
	665	59 (−0.36)	163 (−0.64)
	676	12 (−0.38)	174 (−0.62)
	676	27 (−0.43)	169 (−0.57)

getic with the laser-excited chromophores. (This spectrum is, in fact, only nominally a prompt spectrum, since it is derived by fitting isotropic profiles with convolutions of 5–8 ps fwhm instrument functions with model triexponential decay functions.) Within a very short time (< 2.5 ps in Fig. 7), the spectrum becomes dominated by strong photobleaching and stimulated emission at wavelengths of 675 nm or more – which is consistent with excitation equilibration, primarily into the lowest-energy pigments in LHC-II. Hence, the decay in the prompt photobleaching peak that occurs in the bipolar absorption transient under 650 nm excitation in Fig. 6 arises from downhill energy transfer from the Chl *b* spectral components that absorb at 650 nm. The accentuated fast photobleaching decay observed at 665 nm under 665 nm excitation has a similar origin, as does the gradual attenuation in the fast component's amplitude as the probe wavelength is increased from 665 to 675 nm. Some spectral equilibration persists for delay times longer than 10 ps in Fig. 7, where the zero-crossing wavelength (662–663 nm) between the ESA and photobleaching regions experiences a time-dependent red shift. In contrast, this zero-crossing wavelength exhibits a dynamic blue shift in the difference spectra obtained under 680 nm excitation (not shown), indicating that some uphill spectral equilibration occurs upon excitation at the extreme red edge in the LHC-II absorption spectrum. The absorption transients for this excitation wavelength (not shown) show little of the bipolar behavior in Fig. 6. The profiles for all probe wavelengths between 640 and 655 nm, for example, are dominated here by ESA at all times (Table IV). This is consistent with the interpretation of the spectral evolution in Figs. 6 and 7 in terms of spectral equilibration, since under 680 nm excitation the laser-prepared LHC-II state(s) resemble the 300 K Boltzmann equilibrium more closely than the states prepared under 650 or 665 nm excitation.

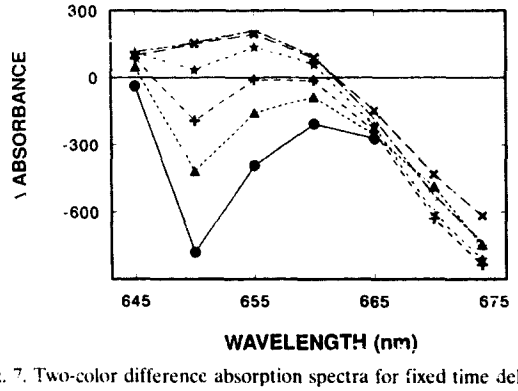

Fig. 7. Two-color difference absorption spectra for fixed time delays, reconstructed from isotropic time-dependent profiles at seven wavelengths from 645 to 675 nm. Excitation wavelength is 650 nm, in the Chl *b* absorption region. Time delays are 0 ps (●), 2.5 ps (▲), 5 ps (+), 10 ps (*), 20 ps (○) and 50 ps (×). Absorption differences are in arbitrary units.

We emphasize that the prompt 650 nm photobleaching band observed under 650 nm excitation in Fig. 7 is not a coherent coupling artifact, which cannot occur when the pump and probe pulses are derived from independent dye lasers. Moreover, the sum frequency detection mode in our multiple modulation scheme precludes scattered pump light from contributing to the difference spectrum, even when the pump and probe wavelengths coincide.

When the pump and probe wavelengths are separated by at least 20 nm, the anisotropies observed in two-color experiments show no resolvable decay under our experimental resolution, unlike the one-color anisotropies at 665–675 nm (cf. Fig. 4 and Table III). The prompt anisotropies, observed at times immediately following the instrument function, are essentially the same as the residual anisotropies $r(\infty)$ measured at long times. Several of these values are contrasted in Table V with the corresponding residual anisotropies measured in the one-color experiments. For probe wavelengths between 640 and 650 nm, the residual

TABLE V

Residual anisotropies observed in one-color and two-color experiments

Pump wavelength λ_2 is 675 nm in all two-color measurements.

Probe wavelength λ_1	One-color $r(\lambda_1, \lambda_1)$	Two-color $r(\lambda_2, \lambda_1)$
640	-0.01 ± 0.03	0.11 ± 0.02
645	-0.03 ± 0.13	0.16 ± 0.02
650	-0.03 ± 0.03	0.23 ± 0.02
675	0.00 ± 0.03	-

anisotropies are considerably larger in the two-color than in the one-color experiments. This interesting feature is rationalized in the light of room-temperature LHC-II linear dichroism spectra in the discussion.

Risetime behaviors were compared in the two-color isotropic signals for LHC-II and oxazine 725 in ethylene glycol, with the results shown in Fig. 8. These signals were probed at 645, 665, 670, and 675 nm under 650 nm excitation. At these probe wavelengths, the oxazine 725 transient absorption arises principally from photobleaching and stimulated emission. The risetime behavior in this dye (which is limited by vibrational equilibration) is essentially prompt under present time resolution. In each case, the risetime of the LHC-II signal essentially parallels that of oxazine 725, indicating that most of the excitation redistribution among LHC-II spectral forms occurs within the two-color instrument function fwhm of 5–8 ps for this excitation wavelength. (However, the absorption difference spectra in Fig. 7 show that some slower spectral equilibration does occur.) The delay of approx. 5 ps between the

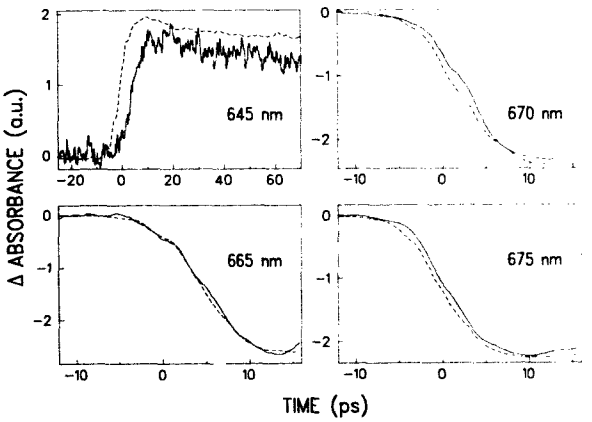

Fig. 8. Comparison of two-color absorption difference risetimes between LHC-II (solid curves) and control solution of oxazine 725 dye in ethylene glycol (dashed curves). Pump wavelength is 650 nm in all cases; probe wavelengths are 645, 665, 670 and 675 nm. The oxazine 725 signal is photobleaching/stimulated emission at all probe wavelengths; the LHC-II signal is dominated by photo-bleaching/stimulated emission at the three longer wavelengths, and by excited state absorption at 645 nm. The oxazine signal at 645 nm is inverted.

645 nm oxazine and LHC-II profiles in Fig. 8 may arise from the disappearance of a prompt photobleaching component in LHC-II at this wavelength.

Discussion

The present LHC-II work is striking in that it confirms seemingly contradictory features in both the earlier one-color pump-probe experiments [10,11] and the fluorescence upconversion study [12]. In particular, Gillbro et al. [10] reported a one-color Chl *b* isotropic signal at 652 nm that decayed with a lifetime of 6 ± 4 ps. This corresponds most closely to our 650 nm signal in Fig. 2, in which a prompt photobleaching signal is supplanted within 4–5 ps by ESA. In this case, the small ESA signal we observe at long times (Fig. 2) may have been obscured by a lower S/N in the earlier work. Our 665 nm anisotropy decay (Fig. 4) qualitatively resembles the one described by Gillbro et al. [10], in that it contains a lifetime component that is easily resolved from our 2–3 ps fwhm instrument function. Our 6.3 ps anisotropic lifetime at that wavelength (Table III) is shorter than their 20 ps depolarization lifetime. Hence, while some details in our one-color experiments differ from those in the earlier pump-probe experiments [10,11], they share a family resemblance with the latter work.

In contrast, our two-color experiments reveal EET dynamics that appear consistent with the subpicosecond energy transfer timescale characterized in the fluorescence upconversion experiments [12]. This is revealed most clearly in the absorption difference spectra in Fig. 7. Here, the bulk of the spectral metamorphosis between the "prompt" and long-time difference spectra occurs within less than 2.5 ps, since by this time the LHC-II photobleaching spectrum has already become concentrated at wavelengths ≥ 675 nm. Additional confirmation appears in the two-color risetime studies in Fig. 8, where the onset of the difference absorption is indistinguishable under the 5–8 ps instrument function from the prompt signal observed in solutions of the control dye oxazine 725. Our two-color anisotropy studies show no evidence for resolvable anisotropy decays, in contrast to the 4–6 ps depolarization lifetimes observed at the longer wavelengths in our one-color experiments. This is consistent with the fluorescence upconversion result of Eads et al. [12], who report an anisotropy decay time of less than 1 ps for fluorescence excited at 650 nm and monitored at 690 nm. Consequently, the major differences between the earlier pump-probe and fluorescence upconversion studies may stem from contrasting projections of EET dynamics viewed in one-color and two-color studies, rather than from improvements in laser time resolution or sample isolation protocol. The two-color absorption difference spectra in Fig. 7 suggest that the spectral

equilibration occurs over a range of timescales: while the major redistribution of the initial photobleaching and stimulated emission occurs within less than 2.5 ps, perceptible red-shifting of the zero-crossing point persists for as long as 20 ps.

In the crudest model for spectral equilibration, we may consider downhill energy transfer from a single Chl *b* pool to a single Chl *a* pool with rate constant k_1. The energy separation between these pools (which absorb at about 650 and about 676 nm) is about 600 cm^{-1}; the rate constant k_{-1} for the reverse (uphill) energy transfer would then be smaller than k_1 by a factor of ~ 17 at room temperature. In the absence of other energy transfer steps, the time-dependent excited state populations $B(t)$ and $A(t)$ in the respective pools (following excitation of the Chl *b* pool) would then become

$$B(t) = B(0) - m + me^{-(k_1 + k_{-1})t} \tag{4}$$

$$A(t) = m - me^{-(k_1 + k_{-1})t} \tag{5}$$

with

$$m = \frac{k_1 B(0)}{k_1 + k_{-1}}$$

In this limit, the lifetime of the fast, single-exponential Chl *b* decay component (which would be mirrored by a Chl *a* rise component) is essentially $1/k_1$, owing to the large disparity between k_1 and k_{-1}. This model can be generalized by also allowing the Chl *b* and Chl *a* pools to decay independently, with rate constants k_2 and k_3, respectively (e.g., due to annihilation). In this case, the excited-state kinetics of the two pools become biexponential, with empirical rate constants k_α, k_α, k_β given by

$$k_\alpha + k_\beta = k_{-1} + k_1 + k_2 + k_3 \tag{6}$$

$$k_\alpha k_\beta = k_{-1}k_2 + k_1k_3 + k_2k_3 \tag{7}$$

As a practical example, we may set $k_1 = 1\ ps^{-1}$, $k_{-1} = 0.06\ ps^{-1}$, $k_2 = k_3 = 0.05\ ps^{-1}$. This would yield empirical lifetimes $k_\alpha \sim 1\ ps^{-1}$, $k_\beta \sim 0.05\ ps^{-1}$ that closely resemble the individual rate constants for downhill energy transfer and exciton annihilation. Such a situation arises because the time scales for these two processes are so disparate. Hence, observation of a range of timescales for spectral equilibration in the two-color experiments suggests a kinetic scheme that is more complex than energy transfers between two homogeneous pigment pools.

The origin of the differences in the LHC-II kinetics observed in one-vs. two-color experiments remains speculative, owing to uncertainties in the chromophore architecture. While the positions and approximate orientations of the 15 chromophores in an LHC-II monomer have been determined by Kühlbrandt and Wang [7], the Chl *a* and Chl *b* molecules have not been differentiated; the locations of the individual pigments responsible for the spectral components identified in the recent LD and CD studies [8] are still unknown. Approximately four of the nine Chl *a* chromophores in a monomer are believed to contribute to the lowest-energy LHC-II absorption band at 676 nm [8]. If dispersion exists in the separations between pairs of such C676 pigments (as is to be expected in this irregular monomer structure [7]), it would lead to multiexponential decay in the 676 nm one-color anisotropy function – which is controlled mainly by excitation equilibration among the pigments whose absorption dominates at this wavelength. Such a situation is strongly implied by the anisotropy parameters for 675 nm in Table III. While the resolvable anisotropy decay is well described by a lifetime of 4.3 ± 2 ps at this wavelength, the fitted initial anisotropy $r(0)$ is only 0.14 – which is well below the theoretical $r(0) = 0.4$. Hence, faster (likely subpicosecond) decay components are likely to be present within the instrument function, and the total one-color anisotropy decay probably contains a superimposition of picosecond and subpicosecond lifetime components.

The residual anisotropies $r(\infty)$ observed at the shorter wavelengths (Table V) can be directly compared with the static LD spectrum of LHC-II trimers. In the latter case, the reduced linear dichroism $(A_\parallel - A_\perp)/(A_\parallel + 2A_\perp)$ measured in a rotationally symmetric antenna is proportional to $\langle P_2(\cos \beta^\mu) \rangle$. Here β^μ is the angle between the pigment Q_y transition moment and the normal to the plane of the disk-shaped trimer [7], and the average is taken over all pigments absorbing at the pertinent wavelength. In the case of the present absorption difference spectra at 640–650 nm, the signal is dominated by ESA (with absorption coefficient A_1) and likely contains some photobleaching (with absorption coefficient A_0). Hence the total anisotropy $r(\lambda_2, \lambda_1)$ measured using pump and probe wavelengths $8gl_2$ and λ_1, will contain contributions r_1 and r_0 from ESA and photobleaching, respectively, according to [23]

$$r = \frac{A_0 r_0 - A_1 r_1}{A_0 - A_1} \tag{8}$$

If the excitation equilibrates among rotationally equivalent monomers in a trimer, the anisotropy function detected in a pump-probe experiment is related to the transition moment angles β^μ, $\beta^{\prime\prime}$ at the pump and probe wavelengths respectively through [24]

$$r(\lambda_2, \lambda_1) = \tfrac{2}{5}\langle P_2(\cos \beta^\mu) \rangle \left\langle \frac{A_0 P_2(\cos \beta^{\prime\prime}_{\text{bleach}}) - A_1 P_2(\cos \beta^{\prime\prime}_{\text{ESA}})}{A_0 - A_1} \right\rangle \tag{9}$$

TABLE VI

Comparison of reduced linear dichroism with residual anisotropy from pump-probe experiments

λ_1 (nm)	Reduced LD [a]	$\langle P_2(\cos\beta^\mu(\lambda_1))\rangle / \langle P_2(\cos\beta^\mu(\lambda_2))\rangle$ [b]
640	0.25 ± 0.04	−0.1 ± 0.3
645	0.25 ± 0.04	−0.1 ± 0.8
650	0.16 ± 0.04	−0.15 ± 0.15
675	1.00	1.00

[a] Room temperature, normalized to reduced linear dichroism at 675 nm.

[b] Excitation wavelength 675 nm in two-color experiments.

(Eqn (9) allows for the possibility that the ESA and photobleaching transition moment directions differ.) Accordingly, the ratio of anisotropies observed at long times in one-color and two-color experiments at the probe wavelength λ_1 will be

$$\frac{r(\lambda_1, \lambda_1)}{r(\lambda_2, \lambda_1)} = \frac{\langle P_2(\cos\beta^\mu(\lambda_1))\rangle}{\langle P_2(\cos\beta^\mu(\lambda_2))\rangle} \tag{10}$$

For fixed excitation wavelength λ_2, this ratio of one-color to two-color residual anisotropies becomes analogous to the reduced linear dichroism in that it is proportional to $\langle P_2(\cos\beta^\mu(\lambda_1))\rangle$.

The linear dichroism spectrum of LHC-II trimers [8] is dominated at long wavelengths by an intense, positive band at 676 nm, corresponding to Chl *a* pigments with Q_y moments that are nearly parallel to the membrane plane ($\beta^\mu \approx 90°$). At the Chl *b* absorption wavelengths 640–655 nm, the LD signals are far smaller. For example, the 77 K spectrum exhibits a positive band at 640 nm and negative bands at 648 and 657 nm. The relevant Chl *b* Q_y transition moments are thus aligned at angles slightly greater than and slightly less than 54.7° from the disk plane, respectively. For direct comparison with our residual anisotropies, the LD spectrum was obtained at room temperature, with the results shown in Table VI. While there are large uncertainties in the pump-probe anisotropies at the shorter wavelengths, the LD data are qualitatively consistent with the residual anisotropies listed in Tables III and IV. Eqn (10) predicts, for example, that the ratio of one-color to two-color residual anisotropies should scale with the linear dichroism at the probe wavelength λ_1. Since the one-color anisotropies are smaller (by a factor of at least 5) than the two-color anisotropies at 640–650 nm, and since this ratio is defined as unity at 675 nm for $\lambda_2 = 675$ nm, this scaling is, in fact, approximately obeyed (Table VI). The large fractional errors in these ratios at the shorter wavelengths stem from the extremely low values of the one-color anisotropies $r(\lambda_1, \lambda_1)$ observed at these wavelengths (cf. Table V).

The low value (-0.03 ± 0.03) of the one-color residual anisotropy $r(\infty)$ at 650 nm (Table V) differs considerably from the value 0.42 ± 0.05 reported at 652 nm [11]. In view of the preceding analysis, the latter value appears to be inconsistent with the static LD spectrum of our LHC-II trimers. Similarly, our residual anisotropy at 665 nm (0.05 ± 0.04) is much smaller than the reported 0.28 ± 0.04 [11]. These differences may originate in part from structural differences between the LHC-II particles isolated using n-dodecyl β-D-maltoside and Triton X-100.

Conclusions

The principal features of our one-color and two-color pump-probe experiments on LHC-II trimers isolated using *n*-dodecyl β-D-maltoside may be summarized as follows:

(1) Both the isotropic and anisotropic decays show clear evidence for subpicosecond downhill excitation transfer, both in the Chl *b* → Chl *a* transfer processes and in excitation equilibration among the Chl *a* spectral forms. The former conclusion is consistent with that drawn by Eads et al. [12] on the basis of their fluorescence upconversion study.

(2) Our isotropic decays also contain the slower lifetime components 2–6 ps, 14–36 ps, and several hundred picoseconds. The 2–6 ps components are connected with dynamic red-shifting in the Chl *a*/*b* absorption difference spectrum; the comprehensive spectral equilibration in LHC-II thus appears to contain picosecond as well as subpicosecond lifetime components. Such multiphasic equilibration kinetics are to expected, given the dispersion in Chl-Chl separations and orientations [7]. The Chl chromophores in a monomer are organized into upper and lower layers containing eight and seven pigments, respectively; the 2–6 ps lifetime components may arise from excitation transfer between layers. The 14–36 ps components may stem from energy transfer between pigments belonging to different monomers. The origin of the longest lifetime components remains unassigned, pending a more thorough study of the exciton annihilation kinetics.

(3) The anisotropy decays are multiexponential. Subpicosecond components dominate the two-color anisotropies; picosecond components are conspicuous in the one-color anisotropies at the red edge of the Chl *a* absorption region. In the latter case, the initial anisotropy $r(0)$ is generally less than 0.4, so that subpicosecond components exist even in the one-color anisotropies. As in the isotropic decays, this multiphasic behavior is consistent with the irregular structure [7] of the LHC-II antenna. The appearance of picosecond components in the one-color anisotropies is reminiscent of the anisotropy decays reported by Gillbro et al. for Triton X-100 preparations of LHC-II [10].

(4) The values of the long-time anisotropies $r(\infty)$ measured in the one-color and two-color experiments are qualitatively consistent with polarized steady-state excitation spectra [8] and with the linear dichroism spectrum of LHC-II trimers.

Acknowledgements

The Ames Laboratory is operated for the U.S. Department of Energy by Iowa State University under Contract No. W-7405-Eng-82. This work was supported by the Division of Chemical Sciences, Office of Basic Energy Sciences. This research was supported in part by the Dutch Foundations for Chemical Research (SON) and for Biophysics (S.v.B.), financed by the Netherlands Organization for Scientific Research (NWO). J.P.D. was supported by a fellowship from the Royal Netherlands Academy of Arts and Sciences (KNAW).

References

1 Bassi, R., Rigoni, F. and Giacometti, G.M. (1990) Photochem. Photobiol. 52, 1187–1206.
2 Larsson, U.K., Sundby, C. and Andersson, B. (1987) Biochim. Biophys. Acta 894, 59–68.
3 Spangfort, M. and Andersson, B. (1989) Biochim. Biophys. Acta 977, 163–170.
4 Kühlbrandt, W., Thaler, T. and Wehrli, E. (1983) J. Cell Biol. 96, 1414–1424.
5 Kühlbrandt, W. (1988) J. Mol. Biol. 202, 849–864.
6 Kühlbrandt, W. and Downing, K.H. (1989) J. Mol. Biol. 207, 823–828.
7 Kühlbrandt, W. and Wang, D.N. (1991) Nature 350, 130–134.
8 Hemelrijk, P.W., Kwa, S.L.S., Van Grondelle, R. and Dekker, J.P. (1992) Biochim. Biophys. Acta 1098, 159–166.
9 Haworth, P., Tapie, P., Arntzen, C.J. and Breton, J. (1982) Biochim. Biophys. Acta 682, 152–159.
10 Gillbro, T., Sundström, V., Sandström, A., Spangfort, M., and Andersson, B. (1985) FEBS Lett. 193, 267–270.
11 Gillbro, T., Sandström, A., Spangfort, M., Sundström, V. and Van Grondelle, R. (1988) Biochim. Biophys. Acta 934, 369–374
12 Eads, D.E., Castner, E.W., Alberte, R.S., Mets, L. and Fleming, G.R. (1989) J. Phys. Chem. 93, 8271–8275.
13 Engh, R.A., Petrich, J.W. and Fleming, G.R. (1985) J. Phys. Chem. 89, 618–621.
14 Van Metter, R.L. (1977) Biochim. Biophys. Acta 462, 642–658.
15 Shepanski, J.F. and Knox, R.S. (1981) Isr. J. Chem. 21, 325–331.
16 Gülen, D. and Knox, R.S. (1984) Photobiochem. Photobiophys. 7, 277–286.
17 Berthold, D.A., Babcock, G.T. and Yocum, C.F. (1981) FEBS Lett 134, 231–234.
18 Van Leeuwen, P.J., Nieveen, M.C., Van de Meent, E.J., Dekker, J. P. and Van Gorkom, H.J. (1991) Photosynth. Res. 28, 149–153.
19 Causgrove, T.P., Yang, S. and Struve, W.S. (1989) J. Phys. Chem. 93, 6844–6850.
20 Lin, S., Van Amerongen, H. and Struve, W.S. (1991) Biochim. Biophys. Acta 1060, 13–24.
21 Becker, M., Nagarajan, V. and Parson, W.W. (1991) J. Am. Chem. Soc., in press.
22 Shepanski, J.F. and Anderson, R.W. Jr. (1981) Chem. Phys. Letts. 78, 165–173.
23 Cantor, C.R. and Schimmel, P.R. (1980) Biophysical Chemistry, Part II, W.H. Freeman and Co., San Francisco.
24 Van Gurp, M., Van Ginkel, G. and Levine, Y.K. (1988) J. Theoret. Biol. 131, 333–349.